Heat partition in edge trimming of fiber reinforced polymer composites

Sheikh-Ahmad, Jamal ; Almaskari, Fahad; Hafeez, Farrukh

DOI:
10.1177/0021998320904129

Document Version
Peer reviewed version

Citation for published version (Harvard):
Sheikh-Ahmad, J, Almaskari, F & Hafeez, F 2020, 'Heat partition in edge trimming of fiber reinforced polymer composites', *Journal of Composite Materials*. https://doi.org/10.1177/0021998320904129

Heat partition in edge trimming of fiber reinforced polymer (FRP) composites

Journal:	*Journal of Composite Materials*
Manuscript ID	JCM-19-1071.R1
Manuscript Type:	Original Manuscript
Date Submitted by the Author:	n/a
Complete List of Authors:	Ahmad, Jamal; Khalifa University of Science and Technology - Sas Al Nakhl Campus, Mechanical Engineering Almaskari, Fahad; Khalifa University of Science Technology - Abu Dhabi Campus Hafeez, Farrukh; University of Birmingham Dubai
Keywords:	Heat partition; FRPs; Temperature distribution; Surface texture
Abstract:	Thermal loading of fiber reinforced composites during traditional machining is inevitable. This is due to the fact that most of the mechanical energy utilized in material removal is converted into heat, which is subsequently dissipated into the workpiece, the cutter and is carried away by the chips. Heat conduction into the workpiece during machining might cause thermal damage due to matrix softening and decomposition if the generated temperatures exceeded the glass transition temperature of the epoxy resin. In this work, the amount of heat flux applied to the machined edge and the temperature distribution in multidirectional CFRP and GFRP composite laminates was determined using an iterative inverse heat conduction method. The transient heat conduction problems in the laminate and cutter were simulated independently using the finite element method and the amount of heat flux applied to each was determined. It was also found that the heat flux conducted to the workpiece represented only a small fraction of the total heat and is more influenced by the feed speed than the spindle speed. The temperature of the machined surface was estimated and correlations with the resulting machined surface texture were made.

Heat partition in edge trimming of fiber reinforced polymer (FRP) composites

Jamal Sheikh-Ahmad [a,*], Fahad Almaskari [b], Farrukh Hafeez [c]

[a] Department of Mechanical Engineering, Khalifa University of Science and Technology, SAN Campus, Abu Dhabi, United Arab Emirates

[b] Department of Aerospace Engineering, Khalifa University of Science and Technology, Main Campus, Abu Dhabi, United Arab Emirates

[c] University of Birmingham Dubai, Block 2, DIAC, Dubai, 341799, United Arab Emirates

Abstract

Thermal loading of fiber reinforced composites during traditional machining is inevitable. This is due to the fact that most of the mechanical energy utilized in material removal is converted into heat, which is subsequently dissipated into the workpiece, the cutter and is carried away by the chips. Heat conduction into the workpiece during machining might cause thermal damage due to matrix softening and decomposition if the generated temperatures exceeded the glass transition temperature of the epoxy resin. In this work, the amount of heat flux applied to the machined edge and the temperature distribution in multidirectional CFRP and GFRP composite laminates was determined using an iterative inverse heat conduction method. The transient heat conduction problems in the laminate and cutter were simulated independently using the finite element method and the amount of heat flux applied to each was determined. It was also found that the heat flux conducted to the workpiece represented only a small fraction of the total heat and is more influenced by the feed speed than the spindle speed. The temperature of the machined surface was estimated and correlations with the resulting machined surface texture were made.

Keywords: Heat partition; FRPs; Temperature distribution; Surface texture.

** Corresponding author: Department of Mechanical Engineering, Khalifa University of Science and Technology, SAN Campus, Abu Dhabi, United Arab Emirates. E-mail: jamal.ahmad@ku.ac.ae.*

1. Introduction

Thermal energy in conventional material removal processes arises from the conversion of mechanical energy into heat. Practically, most of the mechanical energy spent in removing the material is converted into thermal energy [1]. This takes place primarily in two regions, namely the chip formation region and the sliding friction region between the cutting tool and the workpiece and chip contact surfaces. In machining fiber reinforced polymer (FRP) composites, and due to the absence of any considerable plastic deformation, the mechanical energy for chip formation is consumed in fracturing the fibers and the matrix, creating new surfaces and overcoming friction at the inerfaces. The thermal energy generated is then diffused from these regions to the tool and workpiece and is carried away by the chips. The amount of thermal energy diffused into each one of these regions causes its temperature to rise significantly and would eventually lead to adverse effects on its mechanical and physical properties. Temperature rise of the epoxy polymer matrix for example might cause it to soften and decompose by pyrolysis, leading to disintegration of the bond between the matrix and fibers and the subsequent reduction in strength and stiffness of the composite material. Inoue and Hagino [2] and Delahaigue et al. [3] reported small reductions in the fracture toughness and tensile strength, respectively, of CFRP after milling. Furthermore, Halim et al. [4] showed that the glass transition temperature of the polymer epoxy has decreased after machining. On the other hand, temperature rise of the cutting tool causes reduction in its hardness, and thus accelerates tool wear. Tool wear in machining FRPs generally occurs by dislodging of the hard phase from the cutting edge due to selective removal of the softer binder phase as shown by Sheikh-Ahmad and Bailey [5]. The increase of cutting tool temperature lowers the strength of the binder phase and facilitates its removal. Weinert and Kempmann [6] demonstrated that drilling of GFRP with the application of coolant significantly reduces tool wear. Similarly, Khairusshima et al. [7] showed that cutting temperatures and tool wear decreased when chilled air cooling was used during milling CFRP. Lastly, temperature rise of the chips causes them to become tacky due to the softening of the epoxy binder. The heated chips tend to adhere to the chip evacuation surfaces of the cutter leading to further increases in the cutting forces and cutting temperatures.

Current understanding of the heat partition in machining FRPs is not as well established as in conventional metal machining, and only a few attempts were made to investigate this problem in

the past. König and Graß [8] utilized a simple calorimetric calculation to estimate the heat partition in drilling CFRR, GFRP and AFRP. It was reported that more than 50% of the total thermal energy was conducted by the tool and that the greater portion of the reamining heat was evacuated by the chips. Liu et al. [9] established the heat partition into the workpiece for helical machining of CFRP using the conjugate gradient inverse heat conduction method. The material removal process was divided into milling (by the tool periphery) and drilling (at the bottom of the tool). It was concluded that 21% and 18.6% of the heat is evacuated through the workpiece during the milling and drilling processes, respectively. Hintze and Klingelhöller [10] used an inverse heat conduction model to determine the heat partition into the grinding wheel in abrasive circular cutting of unidirectional CFRP. It was shown that the heat partition into the tool falls in the range from 23 to 37% for the 0^o fiber orientation laminate and between 20 and 50% for the 90^o fiber orientation laminate. The heat partition was greatly influenced by the immersion depth of the circular abrasive cutting tool. Wang et al. [11] determined the heat partition in orthogonal cutting of UD-CFRP using analytical and numerical simulation methods and determined that most of the thermal energy was conducted to the workpiece and the chips. The heat partition varied with both fiber orientation and depth of cut, with the largest partition (>96%) shown for the 90 and 135^o fiber orientation laminates. However, these findings seem to be in great disagreement with the previous works. Most recently, Sheikh-Ahmad et al. [12] utilized an iterative inverse heat conduction method to estimate the heat partition in edge trimming operation of CFRP. The heat partition ratios into the workpiece, tool and chips were found to be 7%, 56% and 37%, respectively. These ratios are is in close agreement with the findings in ref. [8,9].

On the other hand, more investigations are found on techniques for measuring the temporal and spatial temperature distributions in the workpiece or cutting tool during machining. Obviously, the most serious challenge in these attempts was the limited accessibility to areas where the temperature gradients are the highest. Nevertheless, the findings in these studies helped in establishing relationships between process parameters and cutting temperatures and provided reasonable estimates of the maximum temperatures which might occur. Kerrigan et al. [13] and Ghafarizadeh et al. [14] used wireless temperature measurement systems to measure the temperatures of the rotating tool in milling CFRP with a burr and ball-end cutters, respectively.

Yashiro et al. [15] measured cutting temperatures during the end and slot milling of CFRP using three different methods, namely tool-workpiece thermocouple method, embedded thermocouples (TC) and infrared thermography (IR). Wang et al. [16] also utilized the tool-workpiece thermocouple technique to measure the interface temperatures in the cutting region by embedding a constantan foil in the CFRP laminate layup and measuring potential difference between the constantan foil and the CFRP. Embedded thermocouple techniques were also used to measure the temperature of the workpiece in close proximity to the cutting zone by other authors. An et al. [17] utilized embedded open thermocouple wires in orthogonal cutting of UD-CFRP. During cutting, the tool would eventually cut the TC wires and close the electric circuit. It was reported that the cutting temperatures were the highest for the 90^o fiber orientation. The cutting temperatures increased with an increase in the cutting speed and an increase in the depth of cut. Jia et al. [18] embedded twisted TC wires in the layup of MD-CFRP and measured the cutting temperatures in end milling. Again, the cutter was allowed to cut the TC wires in order to measure the temperatures at the machined surface. Furthermore, the enhanced resolution and response time of modern infrared thermographic systems provided a good solution for measuring the temperature distribution on accessible surfaces during cutting. Inoue and Hagino [2] measured the temperature on different cutting tools during milling CFRP and reported that a PCD cutter attained the lowest temperature in comparison with coated and uncoated HSS and WC tools. Merino-Perez et al. [19] utilized surface mounted TC and IR thermography to measure the temperatures near the edge of exit hole in drilling CFRP and concluded that IR thermography provided better results due to its high response time. Giasin and Ayvar-Soberanis [20] also measured the temperatures of the exit hole during drilling CFRP/Al stacks and reported that the maximum drilling temperature increases with an increase in the feed speed.

This current study is an attempt to address the complete heat partition problem in fiber reinforced epoxy composites subjected to an edge trimming operation. Both GFRP and CFRP quasi-isotropic laminates are considered. The amount of heat evacuated by the workpiece and cutter was estimated using an inverse heat conduction method. The transient and direction dependent heat condition problems in the workpiece and cutter were modeled independently using the finite element method. A uniform moving heat source was applied to the workpiece in order to represent the energy source from machining. Boundary temperatures on the workpiece surface

were measured with surface mounted thermocouples and used to calibrate the finite element method. The cutter temperature was measured by infrared thermography and the average temperature was used to calibrate the finite element model of the cutter. The amount of heat carried away by the chips was determined by solving the complete heat partition problem.

2. Energy Conversion in Edge Trimming Operation

It is widely accepted that most of the mechanical power spent in machining is converted into heat, which is then partitioned by conduction, convection and radiation into four regions, namely the workpiece ($\dot{Q}_w$), cutter ($\dot{Q}_t$), chips ($\dot{Q}_c$) and the environment ($\dot{Q}_e$). The energy partition equation in machining is therefore expressed as,

$$eP_m = \dot{Q} = \dot{Q}_w + \dot{Q}_t + \dot{Q}_c + \dot{Q}_e \qquad (1)$$

where e represents the efficiency of conversion, which is typically greater than 95% [1]. The amount of energy absorbed by the environment through convection, thermal radiation and thermal conduction is generally low and can be neglected. The heat partition case for edge trimming operation is shown schematically in Figure 1. The mechanical power, P_m can be determined by directly measuring the spindle torque and rotation speed, or indirectly by measuring the spindle electric power, P_e. The instantaneous mechanical power consumed by the cutting process is calculated by the expression,

$$P_m(t) = M(t) \cdot \omega + F_y(t) \cdot v_f = \frac{2\pi NM(t)}{60} + F_y(t) \cdot v_f \qquad (2)$$

where M is the spindle torque, ω is the spindle speed in rad/s, F_y is the feed force and v_f is the feed speed in m/s. The total mechanical energy is determined by the integration of equation (2) over time,

$$P_m = \frac{2\pi N}{60}\int_{t_o}^{t} M(t)dt + v_f\int_{t_o}^{t} F_y(t)dt \quad (3)$$

The first term in eq. (3) represents the power consumed by the cutting action and the second term represents the power consumed by the feed motion. In most cases, the feed speed is very small

when compared to the rotational speed and the second term can be neglected. Alternatively, assuming an efficiency ε for the spindle electric motor, the mechanical power can be determined by the relationship,

$$P_m = \varepsilon \cdot P_{el} \qquad (4)$$

The study of heat partition in machining starts with a known magnitude of the mechanical power, which is converted into heat as indicated by eq. (1). In the present study, machining power is determined by measuring the spindle electric power and using eq. (4) where ε is assumed to be 0.80. The thermal energies $\dot{Q}_w$ and $\dot{Q}_t$ are determined numerically and independently using an iterative inverse heat conduction method, and finally $\dot{Q}_c$ is determined by solving the total heat partition equation (1) assuming $\dot{Q}_e = 0$.

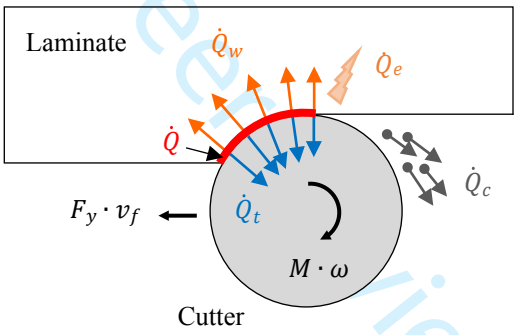

Figure 1. Heat partition is edge trimming operation.

3. Materials and Experimental Methods

Edge trimming experiments were conducted on a 3-axis CNC router to generate data for machining power and boundary temperatures. Figure 2 shows a schematic of the experimental setup where a 500 mm long fiber reinforced polymer (FRP) laminate was clamped to the machine table so that the long side can be trimmed along the edge in a climb cutting configuration. The spindle speed and feed speed utilized were varied according to the parameters shown in Table 1, while the radial depth of cut was kept constant at 5mm (half of the cutter diameter). Two types of FRP material were used, namely carbon fiber reinforced epoxy polymer

composite (CFRP) and glass fiber reinforced epoxy polymer composite (GFRP). The CFRP laminate was 10mm thick and made of twill-weave (2/2) standard modulus carbon fibers with the fiber orientation [0/90^o] and fiber volume fraction of approximately 60%. The GFRP laminate was 8.25 mm thick and made of plain-weave E-glass fibers with the fiber orientation [0/90^o] and fiber volume fraction of approximately 40%. The cutter used was a 2-straight flute PCD milling tool with 10mm diameter, 100 mm total length and 15 mm flute length. The rake and clearance angles of the cutting edge were 0 and 15^o, respectively, and the initial edge radius was 12 μm. Electric power required for machining was measured by a Load Control fast response power meter wired in line with the spindle motor. The net electric cutting power was calculated as the difference between the average spindle power during cutting and idling. Measurements of boundary temperatures were made by thermocouples mounted on the top surface of the laminate, approximately halfway as shown in Figure 2. This allowed for the temperatures to reach steady state by the time the cutter passed by the thermocouples. Gage 36, type K sheathed thermocouples were used. Thermocouple beads were placed in 1.0 mm diameter, 1.5 mm deep holes drilled on the top surface at specific locations from the machined edge. The holes were filled with thermal conductive paste before inserting the thermocouple wires. A Fluke Ti400 thermographic camera was used to capture the temperature of the cutter. The camera was placed about 500 mm away from the edge of the laminate and was focused on the cutting zone. A special suction shroud was mounted around the cutter and allowed effective chip evacuation for a clear image capture of the cutter. As the cutting tool passed by the field of view of the camera, thermal images were captured at a speed of one frame every three seconds, which is the maximum sampling speed of the camera. The IR images thus obtained were analyzed using Smart View software. The temperature recorded by the infrared camera was adjusted for the emissivity of the tool and an average tool temperature was estimated over a rectangular area overlapping the exposed surface of the tool as shown in Figure 6. The emissivity of the tool was determined experimentally using the black body calibration method and was found to be 0.87. Quality of the machined surfaces was evaluated by a non-contact white light metrology system (Alicona InfiniteFocus G5).

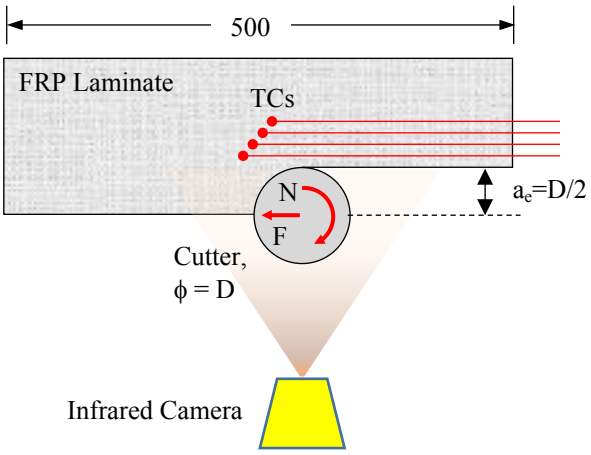

Figure 2. Setup for edge trimming experiment.

Table 1. Experimental conditions

Parameter	**Values**
Spindle speed, rpm	4000, 8000
Feed speed, mm/min	400, 800
Feed per tooth (mm/z)	0.025, 0.05, 0.10

4. Inverse Heat Conduction Method

Inverse heat conduction methods can be used to determine the heat flux on an inaccessible surface by measuring the temperatures on an accessible boundary. In edge trimming operation, the machined surface in contact with the cutting tool is inaccessible, as shown in Figure 1 and direct measurement of its temperatures is not possible. To facilitate the evaluation of the heat flux applied to each element of the edge trimming system, the tool and laminate are separated and modeled independently. For each one of these elements, the boundary temperatures on accessible surfaces were measured and used to determine the corresponding applicable heat flux using the inverse heat conduction method, as explained below.

4.1 Numerical model of the FRP laminate

Figure 3 shows the heat transfer model used to simulate edge milling of FRP laminates. The heat diffusion problem in the workpiece is 3-D nonlinear and transient, and in the absence of internal heat generation is represented by the heat conduction equation:

$$\frac{\partial}{\partial x}\left(k_x(T)\frac{\partial T}{\partial x}\right)+\frac{\partial}{\partial y}\left(k_y(T)\frac{\partial T}{\partial y}\right)+\frac{\partial}{\partial z}\left(k_z(T)\frac{\partial T}{\partial z}\right)=\rho c(T)\frac{\partial T}{\partial t} \quad (5)$$

The boundary conditions applied to the laminate are as shown on the figure and the initial condition for the problem is set as $T(x,y,z,t)=T_o$, at t = 0. The heat transfer coefficients on the machined surface and the top surface were set higher than the bottom surface ($h_1>h_2$) because these two surfaces were subjected to more air movement due to the suction from the dust collector and the rotating tool. The heat transfer coefficients used in the current simulation were determined by trial and error as h_1 = 100 W/°K.m^2 and h_2 = 50 W/°K.m^2. Thermal properties of the quasi-isotropic workpiece were assumed to be directional and temperature dependent. Their values are shown in Tables (2) and (3) for the CFRP and GFRP materials, respectively. The moving heat flux was assumed to be uniformly distributed over the projected area of contact between the cutter and the workpiece, which was assumed to be flat and 5mm in width (equal to the tool radius) and height equal to laminate thickness. During model development, linear heat flux distribution was also tried and found to have negligible effect on the results. DFLUX user subroutine was utilized to introduce the moving heat flux in the numerical simulation. The magnitude of heat flux was determined by minimizing the objective functions in equations (6) and (7) over time and space domains, respectively:

$$SSE1=\sum_{i=1}^{n}\sum_{t=1}^{m}(Y_i(t)-T_i(t))^2 \quad (6)$$

$$SSE2=\sum_{j=1}^{l}\sum_{x=1}^{k}(Y_j(x)-T_j(x))^2 \quad (7)$$

where Y_i is measured temperature history and T_i is simulation temperature history for thermocouple location i and Y_j is the measured peak temperature and T_j is the simulated peak temperature at location x for thermocouple location j.

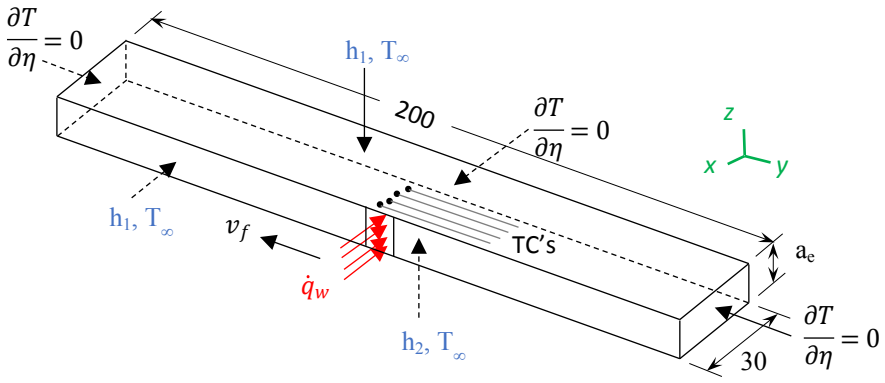

Figure 3. Numerical model of the workpiece.

The element type used for the workpiece was DC3D8 (thermal analysis), a 3D 8-noded linear heat transfer brick type element, and 60000 elements and 68541 nodes were used. Fine mesh with element size 1x1x0.25mm^3 was used in the steep thermal gradient region and a coarse mesh of size 1x1x2.5mm^3 was used for the remaining regions. Convergence of the numerical solution was determined by adjusting the time increment implemented in Abaqus solver. It is was determined that a time increments of 0.01 second guaranteed a converging solution with adequate accuracy [12].

Table 2. Material properties of CFRP [21]

Property	**Units**	**T = 297 °K**	**T = 473 °K**
ρ	g/cm^3	1.550	1.550
k_x, k_y	W/m-°K	2.40	3.00
k_z	W/m-°K	0.60	0.66
c	J/g-°K	0.820	1.320

Table 3. Thermal properties of the GFRP [22]

Property	**Units**	**T=300 °K**	**T=423 °K**
ρ	g/cm^3	1.570	1.570
k_x, k_y	W/m-°K	0.89	0.89
k_z	W/m-°K	0.39	0.39
c	J/g-°K	0.888	1.301

4.2 Numerical model for the tool

The heat diffusion problem in the cutter was also described by a transient nonlinear expression,

$$\nabla \cdot k\nabla T = \rho c \frac{\partial T}{\partial t} \qquad (8)$$

subject to the boundary conditions as shown in Figure 4 and having the initial condition: $T(r,\theta,z,t) = T_o$, at t = 0. The numerical model for the cutter consisted of a cylindrical body 100 mm in length and 10 mm in diameter. Convection heat loss with heat transfer coefficient h_3 = 1000 W/°k.m^2 was assumed on all exposed surfaces of the cutter due to its very high speed of rotation. The part of heat from machining which was conducted to the cutter, $\dot{q}_t$, was applied only at the points of contact between the cutter and the workpiece over a length a_e, equal to the thickness of the CFRP laminate. Since the cutter rotated at very high speed, the frequency of application of the heat flux on each of the flutes was extremely high and it was reasonable to assume that the heat source in this case as stationary. The magnitude of heat flux was determined by minimizing the objective function in equations (9):

$$E = min\left|T^e_{avg} - T^s_{avg}\right| \qquad (9)$$

where T^e_{avg} is average steady state cutter temperature determined by IR thermography and T^s_{avg} is the simulated average cutter temperature. While this approximation method does not provide a realistic distribution of the tool temperature in the numerical model, it does provide an approximate estimate the heat flux going into the cutter. Thermal properties at room temperature of both PCD and tungsten carbide used in the cutter model are shown in Table 6. Higher temperature properties were not available. The total number of elements and nodes used for the numerical model of the cutter were 34,565 and 10189, respectively. Two element types were used by default, DC3D8 in the cutting region and DC3D4 in the tool shank region. DC3D4 is a 4-node linear heat transfer tetrahedron.

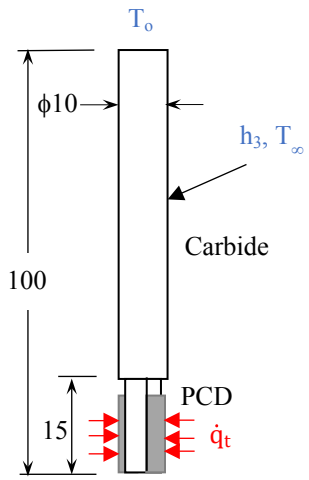

Figure 4. Numerical model for the cutter.

Table 4. Material properties of cutter

Property	Units	PCD	WC-Co
ρ	g/cm³	3.500	15.000
k	W/m-°K	2000	100
c	J/g-°k	0.518	0.130

5. Results and Discussion

5.1 Boundary temperatures

Figure 5 shows typical temperature histories as recorded by surface mounted thermocouples for the CFRP and GFRP laminates during edge trimming at spindle speed of 4000 rpm and feed speed of 800 mm/min. The locations of the hole centers where the thermocouples were inserted are shown between parentheses in the legends. It is noted that the FRP laminate remains at room temperature until the cutter comes in line with the thermocouple array, then the temperature rises abruptly to a maximum before it declines again due to cooling and the cutter moving away. The peaks of the different thermocouples are not coinciding due to lags caused by poor thermal conductivity, slow response of the thermocouples and misalignment of the thermocouple locations from the vertical as shown in figure 2. The highest temperature of 53 ^{o}C was recorded by TC1 at 1.8 mm from the machined edge for the CFRP laminate, while the highest temperature recorded at the same location for the GFRP laminate was 34 ^{o}C. This indicates that a higher heat input was received by the CFRP laminate while machining at the same conditions. It is also

noted that the cooling curve for the CFRP laminate is much steeper than that for the GFRP laminate due to the higher in-plane thermal conductivity as shown in Tables 2 and 3. The temperature peaks and thermal histories obtained from these and similar results are used as boundary temperatures for determining the amount of heat flux conducted to the workpiece as explained in section 5.2.

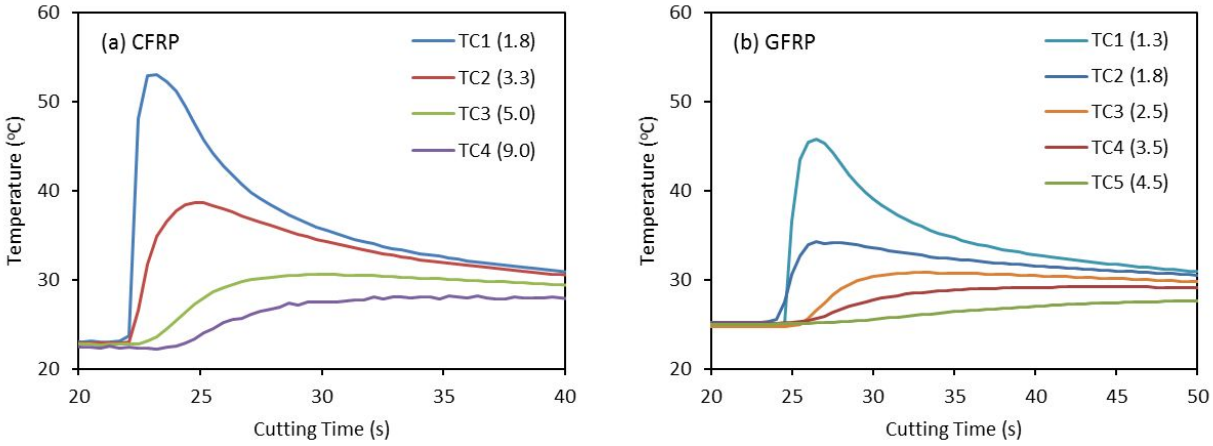

Figure 5. Temperature histories recorded by surface mounted thermocouples when edge trimming at 4000 rpm and 800 mm/min for (a) CFRP and (b) GFRP laminates. Numbers in parentheses indicate TC locations in mm from the machined edge.

Figure 6 shows thermographic images of the cutting zone for the two FRP laminates when edge trimming at 4000 rpm and 800 mm/min. Each image shows three distinctive areas of the cutting zone, namely the cutter, the chips and the machined surface. The temperature profile along a line extending horizontally from one end of the image to the other and running roughly in the middle of the thickness of the machined edge is shown imposed on each image. It is also noted here that the better thermal conductivity of CFRP compared to GFRP produces a smaller spatial temperature gradient. The hottest region in each image is that of the cutter, with the highest temperatures being on the trailing side of the cutter leaving the cutting zone. The maximum temperature of the cutter trimming the CFRP laminate is shown to be 253 °C and that of the cutter trimming the GFRP laminate to be 223 °C. The average cutter temperature is calculated over a square area overlapping the exposed side of the cutter as shown. This average temperature was used as the boundary temperature for minimizing the objective function in eq. (9). The average temperature was used in this context instead of the maximum temperature because of the

great fluctuations in the recording of the maximum temperature over a very small area as shown in the figure.

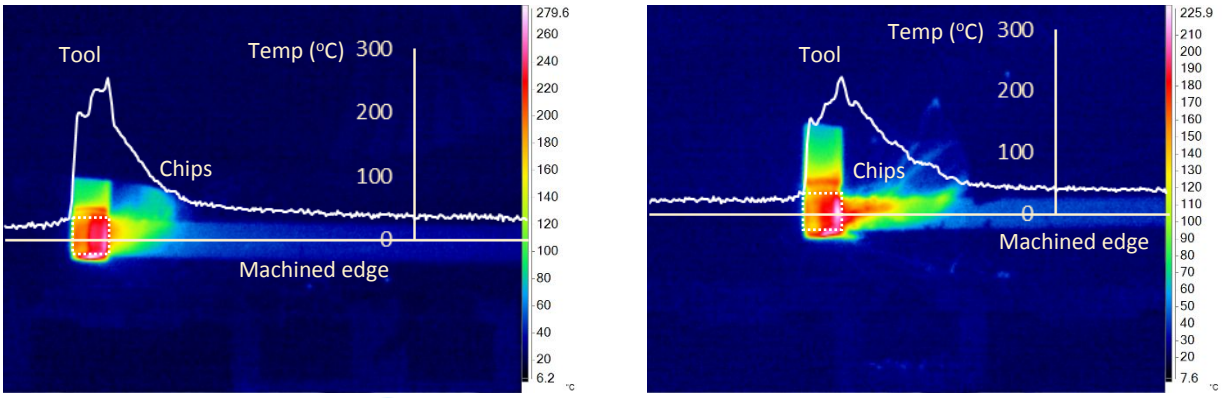

(a) CFRP (b) GFRP

Figure 6. Thermographic images of the cutting zone when edge trimming at 4000 rpm and 800 mm/min for (a) CFRP and (b) GFRP.

Figure 7 shows the average tool temperature for each laminate as a function of the feed per tooth. It is shown that the average tool temperature in cutting CFRP is approximately 40°C higher than that in cutting GFRP. This is due to the higher strength of the CFRP laminate, which translates into higher cutting energy, a portion of which is conducted to the tool. The average cutter temperature changes slightly with cutting conditions. It increased slightly with an increase in the feed speed and an increase in the spindle speed because both increases cause an increase in the machining power as indicated by eq. (2). The increase in feed speed causes an increase in the machining power by increasing the cutting forces due to the larger size of uncut chips. The increase in rotation speed increases the machining power directly. Very few studies reported on the cutter temperature in edge trimming CFRPs. Kerrigan et al. [23] reported that the cutter temperature increases with increasing both feed speed and spindle speed, with the former having the greater effect. Ghafarizadeh [14] reported that the cutter temperature increased with an increase in cutting speed. El-Hofy et al. [24] reported that the cutter temperature increased with an increase in the cutting speed and decreased with the increase in feed per tooth. Both results in [23] and [24] indicated a strong interaction between the cutting speed and feed speed in their influence on cutter temperature.

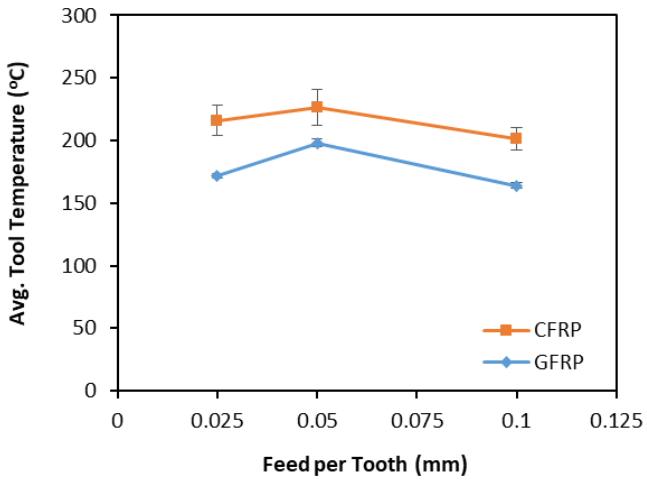

Figure 7. Effect of cutting conditions on the average tool temperature.

5.2 Heat partition into the workpiece

The heat conducting problem for the workpiece was solved numerically for different values of the heat flux $\dot{q}_w$ and different feed speeds. The heat flux conducted to the workpiece was increased systematically in increments of 50 mJ/mm^2·s and the simulated boundary temperatures for each flux value were recorded. The correct magnitude of the heat flux $\dot{q}_w$ for each FRP material at each cutting condition was determined by minimizing the objective functions in equations (6) and (7), which compare the simulated boundary temperatures to the measured ones. Figure 8 shows a comparison between the measured peak temperatures and simulated peak temperatures for both FRP laminates when machining at 4000 rpm and 800 mm/min. It can be seen that the simulated temperature gradient in each cases closely resembles the measured one. The objective function in eq. (7) calculates the square of the difference between the measured and simulated peaks for each value of $\dot{q}_w$ and determines the heat flux corresponding to the minimum difference. Similarly, the objective function in eq. (6) determine the minimum heat flux by comparing measured and simulated temperature histories. The minimum heat flux for each experiment is determined as the average of the heat fluxes determined by both objective functions for all repeats of the same experiment. Once the minimum heat flux is determined, the portion of total heat conducted to the workpiece is determined by multiplying the heat flux by the projected contact area,

$$\dot{Q}_w = \dot{q}_w \cdot A_w \qquad (10)$$

Finally, the energy partition ratio, R_w is determined by dividing the portion of heat conducted to the workpiece by the total power,

$$R_w = \frac{\dot{Q}_w}{\varepsilon \cdot P_{el}} = \frac{\dot{Q}_w}{P_m} \qquad (11)$$

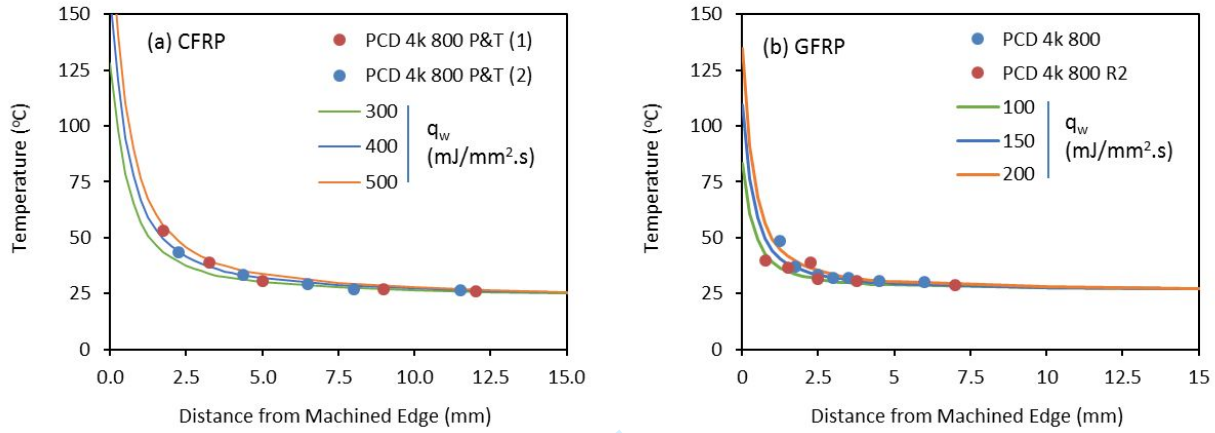

Figure 8. Comparison between measured and simulated peak temperatures at different distances from the machined edge for different levels of $\dot{q}_w$ when edge trimming at 4000 rpm and 800 mm/min.

Figure 9 shows the calculated heat conducted to each laminate as a function of the feed per tooth. Figure 10 shows the partition ratio of this heat to the total heat generated. The error bars on the figure represent the standard deviation of the data obtained at each specific combination of cutting conditions. The large variation in some of the data sets is attributed mainly to uncertainties in the thermocouple measurements and their locations. The main issue with thermocouple temperature measurements is the response time, which might not be short enough to capture the real dynamic response of thermal behavior of the laminate. Nevertheless, the certainty of the results are reasonable for the most part. The heat conducted to the CFRP laminate is much higher in magnitude than that conducted to the GFRP laminate. This is due to the higher heat generated when machining CFRP and the higher heat conductivity of carbon fibers (Tables 2 and 3). The heat conducted to the workpiece appears to increase with an increase in the feed speed and an increase in the spindle speed. Again, this is mainly attributed to the proportional increase in the machining power. The heat partition ratio decreases significantly with an increase in the feed speed for both FRP laminates and its variation with spindle speed is

insignificant (Fig. 10). The main reason for this behavior is exposure time. For slow feed speeds the time available for heat conduction is higher and thus more heat is conducted to the workpiece. Similar findings were reported in [8] in the case of drilling FRPs. It was shown that the heat partition in CFRP was substantially higher than that in GFRP, and in both cases it decreased with an increase in the feed per revolution. It can be noted here that the heat partition ratio for FRPs is relatively small in comparison to those observed in metal cutting. The highest heat partition ratio for CFRP is 0.14 at the smallest feed per tooth and stabilizes at 0.08 for feed per tooth values higher than 0.05 mm. The highest heat partition ratio for GFRP is 0.07 at the smallest feed per tooth and decreases to about 0.04 for higher feeds per tooth. On the other hand, it was shown that the heat partition into the workpiece in the dry milling of steel to vary with undeformed chip thickness from 0.10 to 0.50, with the larger partition ratio associated with the smaller undeformed chip thickness [25]. Luchesi and Coelho [26] determined this partition in face milling of 4340 steel to be 0.35. Both of these works utilized an inverse heat conduction method to determine the heat partition ratio.

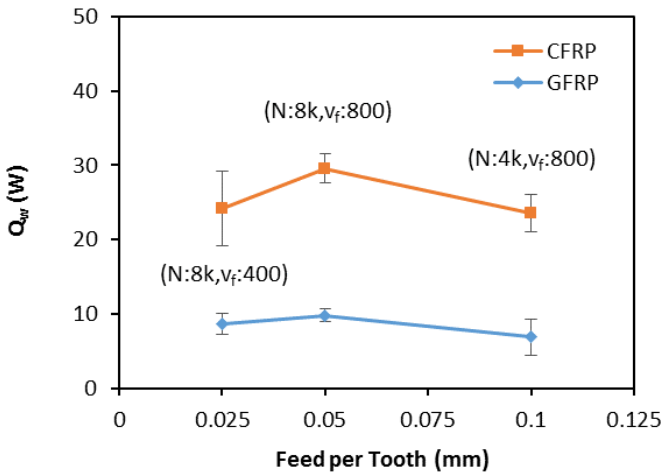

Figure 9. Variation of the heat portion ratio Q_w conducted to the workpiece with cutting conditions.

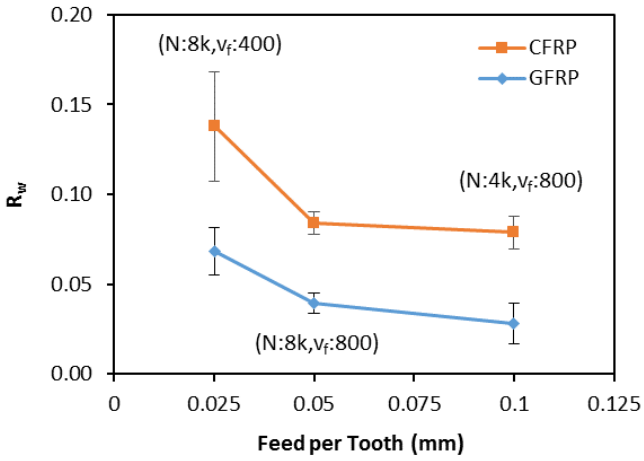

Figure 10. Variation of the heat partition ratio R_w with cutting conditions.

5.2 Heat partition into the cutter

Similarly, the heat flux applied to the cutter, $\dot{q}_t$, was obtained by minimizing the difference between measured and simulated average cutter temperatures as described in sections 4.2 and 5.1. The portion of heat conducted to the cutter, $\dot{Q}_t$ and the heat partition ratio, R_t were then determined by equations (12) and (13), respectively.

$$\dot{Q}_t = \dot{q}_t \cdot A_t \qquad (12)$$

$$R_t = \frac{\dot{Q}_t}{\varepsilon \cdot P_{el}} \qquad (13)$$

Figures 11 and 12 show the variation of the heat conducted to the cutter and heat partition ratio, as a function of the feed per tooth for both FRP laminates, respectively. The behavior of the heat partition into the cutter is similar to that for the workpiece, except that the magnitudes are much higher for the cutter. It is shown that as much as 60% of the heat generated in machining is conducted into the cutter at feed per tooth of 0.025 mm (smallest feed speed). Further increase in the feed speed causes the heat partition ratio to drop to approximately 0.3. Furthermore, the heat partition ratio is slightly higher for the GFRP than the CFRP. Apparently the lower heat conductivity of the GFRP material allowed less heat to be dissipated through the workpiece (Figure 10) and more heat to be dissipated through the cutter. König and Graß [8] also reported

slightly higher heat partition to the tool in the case of drilling GFRP and heat partition ratios in the range from 0.51 to 0.62.

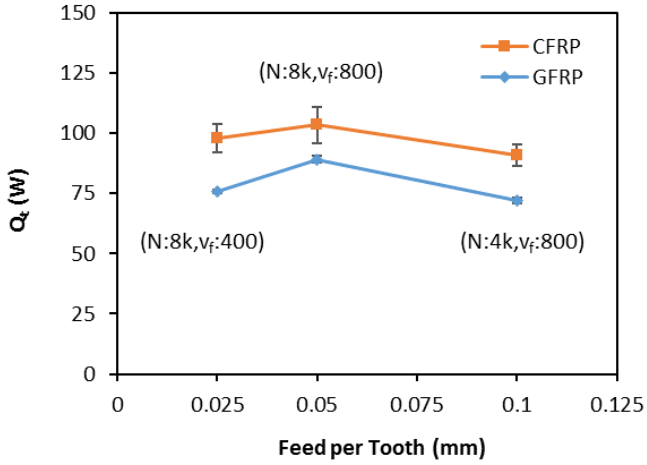

Figure 11. Variation of the heat partition ratio Rw with cutting conditions.

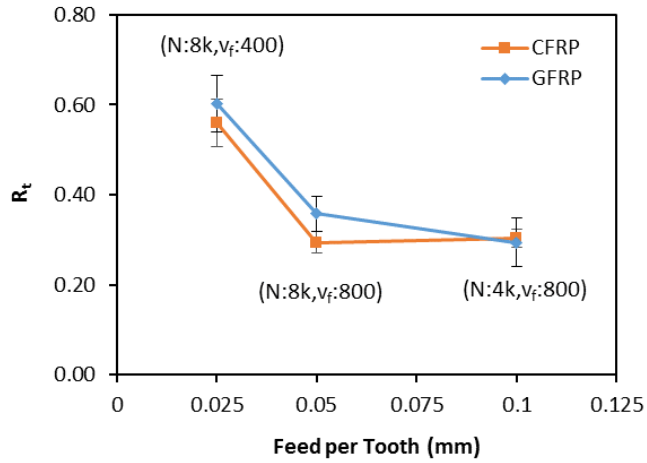

Figure 12. Variation of the heat partition ratio Rw with cutting conditions.

5.3 Total energy balance

The complete heat partition at the cutting zone can now be determined from by eq.(1). Neglecting the heat dissipated to the environment, $\dot{Q}_e$ the heat carried away by the chips is determined by subtracting the values for $\dot{Q}_t$ and $\dot{Q}_w$ from the total heat,

$$\dot{Q}_c = \dot{Q} - \dot{Q}_t - \dot{Q}_w \qquad (14)$$

Similarly, the heat partition ratio for the chips is determined by eq.(15).

$$R_c = \frac{\dot{Q}_c}{\varepsilon \cdot P_{el}} \qquad (15)$$

Figures 13 and 14 show the variation of the heat carried away by the chips and the heat partition into the chips, respectively as a function of the feed per tooth. Tables 5 to 8 list the energy partition and heat partition ratio for both laminate materials as determined by the procedure outlined in the sections above. It is noted here that $R_t + R_w + R_c = 1$. The heat partition into the chips generally increases with the increase in the uncut chip size (feed per tooth). This is expected as larger chips carry more heat than smaller chips. Under the same cutting conditions, the CFRP chips carry more heat than the GFRP chips due to the higher total energy input for the case of CFRP as shown in Tables 5 and 6. The heat partition ratio for the chips does not appear to depend greatly on the fiber material as shown in Figure 14. This is due to the fact that the heat capacities and densities of the two materials are approximately the same. Examining the results in tables 7 and 8, it can be concluded that most of the thermal energy in edge trimming FRPs is dissipated through the cutting tool and chips and that only a small portion of this energy is conducted to the workpiece. A clear change of roles takes place as the feed speed is increased. For the low feed speed, more heat is dissipated through the tool than by the chips (approx. 60% vs. 30%). These ratios are reversed when the feed speed is increased. The effect of spindle speed on the heat partition seems to be insignificant.

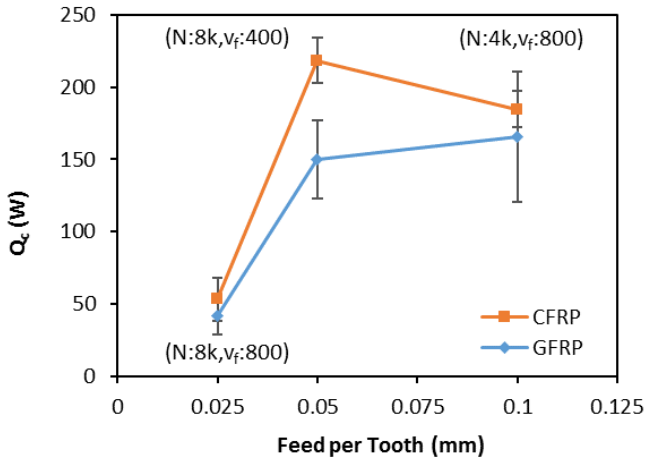

Figure 13. Variation of the heat partition ratio R_w with cutting conditions.

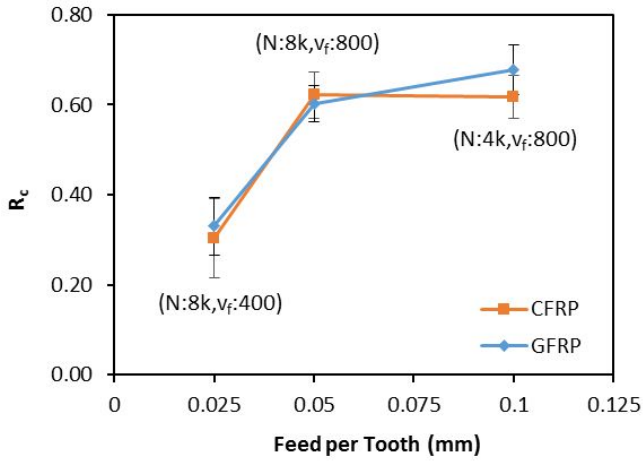

Figure 14. Variation of the heat partition ratio R_w with cutting conditions.

Table 5. Energy partition in edge trimming of CFRP

N (rpm)	v_f (mm/min)	f_z (mm)	P_{el} (W)	$\dot{Q}_w$ (W)	$\dot{Q}_t$ (W)	$\dot{Q}_c$ (W)
8000	400	0.025	219.0±15.6	24.2±5.1	97.9±6.0	53.1±14.7
8000	800	0.05	439.4±17.3	29.6±1.9	103.5±7.5	218.4±15.9
4000	800	0.1	373.8±14.4	23.5±2.6	90.8±4.6	184.7±12.6

Table 6. Energy partition in edge trimming of GFRP

N (rpm)	v_f (mm/min)	f_z (mm)	P_{el} (W)	$\dot{Q}_w$ (W)	$\dot{Q}_t$ (W)	$\dot{Q}_c$ (W)
8000	400	0.025	157.7±16.4	8.6±1.4	75.9±0.85	41.7±13.2
8000	800	0.05	311.1±33.8	9.8±0.9	89.1±1.43	150.0±27.1
4000	800	0.1	305.5±56.6	6.9±2.4	72.0±1.20	165.6±45.3

Table 7. Heat partition ratios in edge trimming of CFRP

N (rpm)	v_f (mm/min)	f_z (mm)	R_w	R_t	R_c
8000	400	0.025	0.138±0.031	0.559±0.053	0.303±0.062
8000	800	0.05	0.084±0.006	0.294±0.024	0.621±0.025
4000	800	0.1	0.079±0.009	0.304±0.019	0.618±0.021

Table 8. Heat partition ratios in edge trimming of GFRP

N (rpm)	v_f (mm/min)	f_z (mm)	R_w	R_t	R_c
8000	400	0.025	0.068±0.013	0.602±0.063	0.330±0.064
8000	800	0.05	0.039±0.006	0.358±0.039	0.603±0.040
4000	800	0.1	0.028±0.011	0.294±0.055	0.677±0.056

5.4 Estimation of machined surface temperature

Figure 15 shows the temperature distribution in the CFRP and GFRP laminates when cutting at 8000 rpm and 400 mm/min (f_z = 0.025mm). These temperature distributions were obtained by applying the estimated heat flux values to the workpiece as described in section 5.2. It can be seen that the heat penetration in the workpiece is very shallow due to the low thermal conductivity of FRPs. The heat penetration and temperature rise in the CFRP is higher than that for the GFRP because of the higher heat flux applied and the higher thermal conductivity. At the cutting zone, the maximum temperature occurs in the region of application of the heat flux just behind the center of the cutter. The maximum machined surface temperature was found to be 233 ^{o}C and 178 ^{o}C for the CFRP and GFRP laminates, respectively. Both temperatures exceed the glass transition temperature of the epoxy matrix, which was reported as 180 ^{o}C by the laminates supplier. Figure 16 shows the estimated maximum temperature on the machined surface for the two laminate materials as a function of the feed per tooth. It can be seen that the machined surface temperature decreases linearly with the increase in the feed per tooth. However, the effect of feed speed on the machined surface temperature seems to be less than the effect of spindle speed. It is apparent that doubling the feed speed caused less temperature change than doubling the spindle speed for both laminate materials. Furthermore, the CFRP laminate machined surface temperature is always about 60 ^{o}C higher than that of the GFRP laminate. These results are in agreement with the findings of Wang et al. [16] were it was reported that the spindle speed was the most influential parameter on the cutting temperatures. The range of machined surface temperatures for the CFRP laminate are also in agreement with those reported in [15].

5.5 Effect of cutting temperatures on machined surface quality

It is apparent on Figure 16 that the maximum temperature on the machined surface for the CFRP laminate exceeds the glass transition temperature of the epoxy matrix for feed per tooth values of 0.025 and 0.05 mm. The estimated maximum surface temperature for the GFRP is close to the glass transition temperature for the feed per tooth of 0.025 mm. Therefore, thermal damage is likely to occur at these conditions due to loss of mechanical properties at and below the surface at these cutting conditions. The machined surface temperatures for the GFRP laminate are all

well below the glass transition temperature of the epoxy polymer for higher feed per tooth values and thermal damage is less likely. The extent of thermal damage below the CFRP machined surface can be estimated from the numerical temperature distribution by determining the heat penetration depth corresponding to the glass transition temperature of 180 °C. Figure 17 shows the estimated depth of thermal damage for the CFRP laminate as a function of the feed per tooth. The heat penetration depth varies almost linearly with the feed per tooth from 0.32 mm at f_z = 0.025mm to 0 mm at f_z = 0.1 mm.

Figure 15. Contours of the temperatures in the machined workpiece for edge trimming at 8000 rpm and 400 mm/min, (a) CFRP and (b) GFRP.

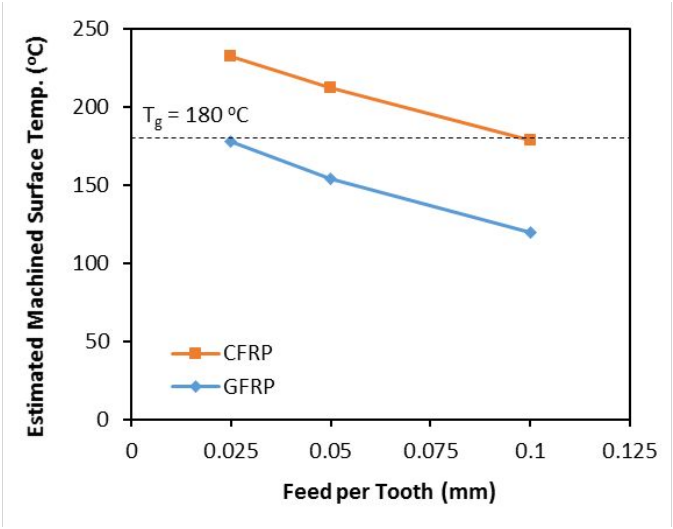

Figure 16. Estimated machined surface temperatures at different cutting conditions for the CFRP and GFRP laminates.

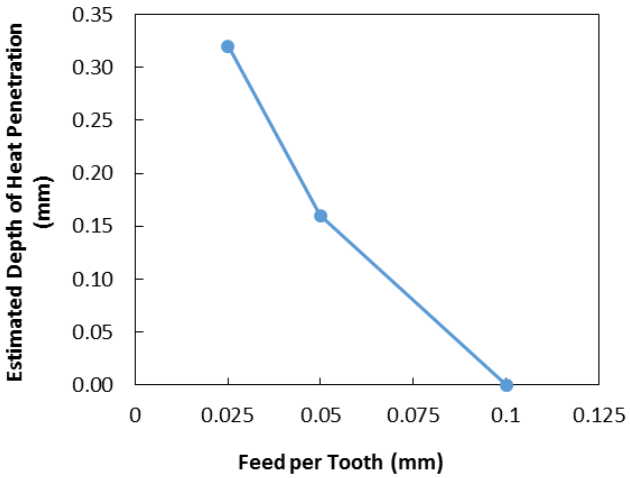

Figure 17. Estimated depth of thermal damage for the CFRP at different cutting conditions.

Figures 18-21 show the surface textures of the machined edge for the different FRPs at the conditions of low and high surface temperatures (i.e. f_z = 0.1 mm and f_z = 0.025 mm, respectively). The figure captions also show the 10 point average height, S10z, for the inspected surface, which is 0.8mmx0.8mm. Each machined surface was inspected at six different locations and the average height, Sa and 10 point average height, S10z parameters were recorded. It was noticed that the surface textures varied greatly from one location to another and between different repeats of the same experiment as well, and the variation was the greatest for the CFRP laminate. Nevertheless, the machined surface roughness as represented by the S10z parameter generally increased slightly with the increase in feed per tooth for CFRP, and decreased with the increase in feed per tooth for the GFRP. This contrast in behavior can be largely attributed to the differences in machined surface temperatures as shown in Figure 16.

The machined surface textures for the CFRP laminate at low and high temperatures did not differ significantly (Figs. 18 and 19). This is perhaps due to the fact that the machined surface temperature was at or above the glass transition temperature for both conditions. A similar observation was also reported by [12]. The machined surface is clearly characterized by two distinct regions, parallel and normal to the surface fiber regions. In the parallel fiber region the

machined surface is relatively smooth and the fibers are clearly visible. On the other hand, the region of fibers normal to the surface show great variation in surface topography as shown by regions A and B marked on the figures. In region A the fibers are clean cut and the fiber ends are clearly visible at high magnification. In region B, the fibers are masked by what appears to be epoxy deposits on the surface. These epoxy deposits appear to occur in resin-rich regions between the weft and fill fiber tows. Furthermore, the greatest variation in surface topography occurred mainly in the normal fibers region. For the low temperature condition, the surface craters are larger in area than those occurring on the high temperature surface. However, they are shallower. These particular surface features might have been the result of high temperature damage of the epoxy matrix.

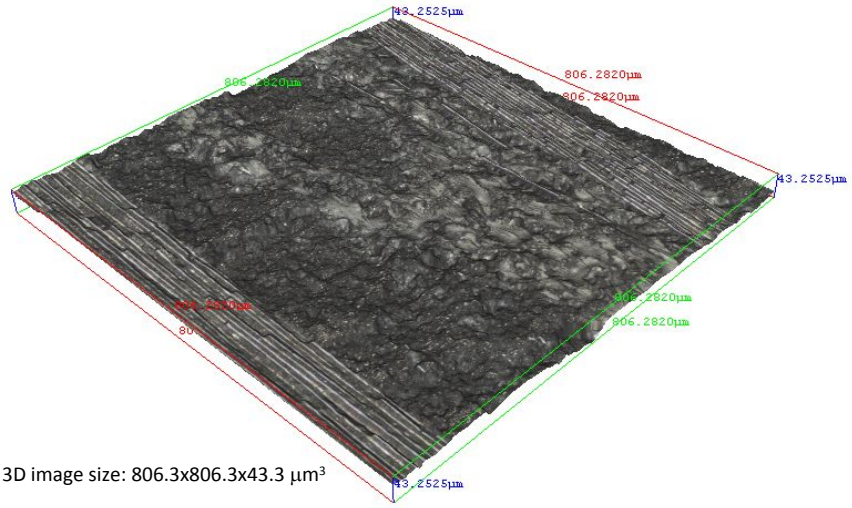

3D image size: 806.3x806.3x43.3 µm^3

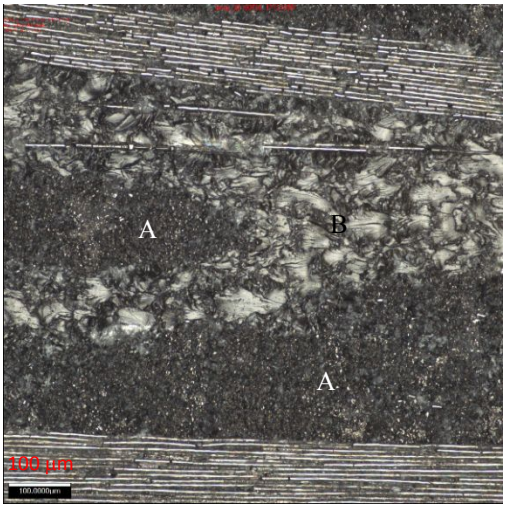

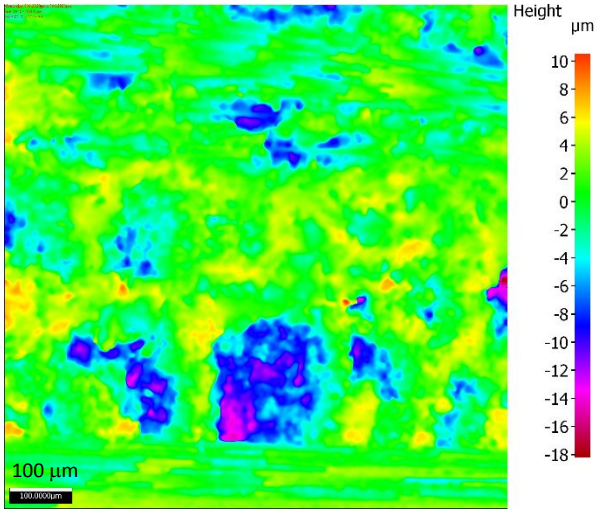

Figure 18. Surface texture of CFRP laminate after machining at 8000 rpm and 400 mm/min (T = 179 °C, S10z = 31.977±4.963 µm).

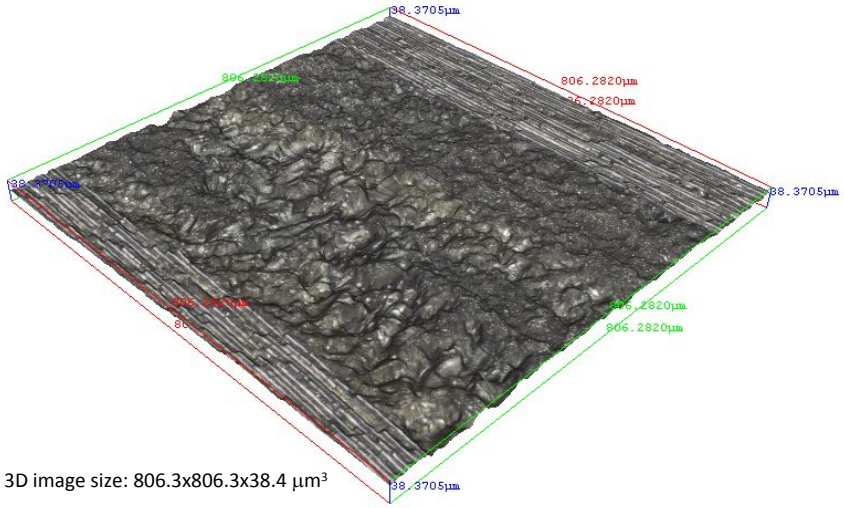

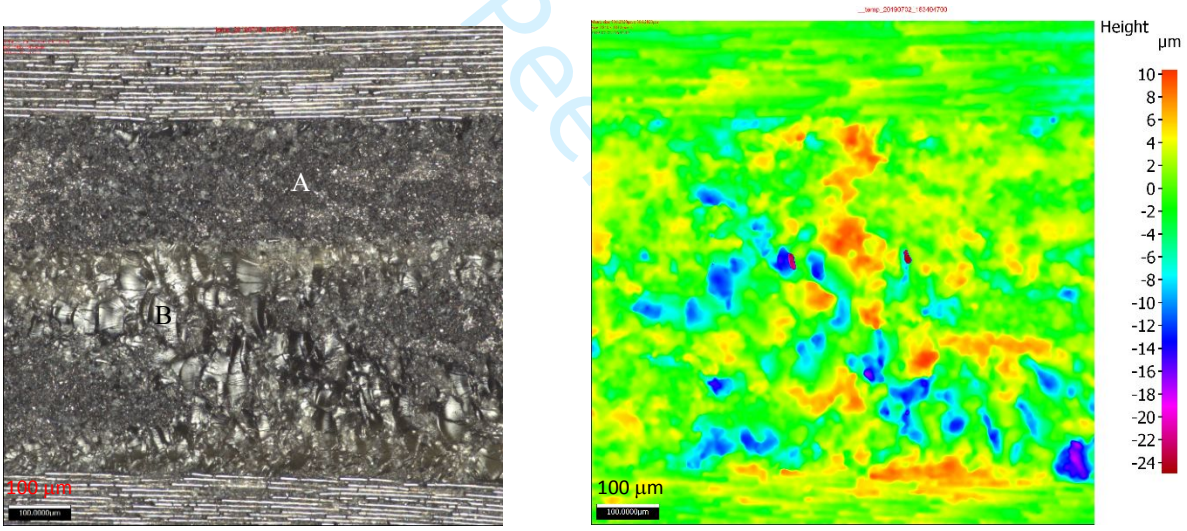

Figure 19. Surface texture of CFRP laminate after machining at 8000 rpm and 400 mm/min (T = 218 °C, S10z = 33.495±5.085 µm).

The machined surface textures for the GFRP laminate at low and high temperatures differ greatly in appearance and magnitude (Figs. 19 and 20). The machined surface at low temperature appears smoother and the surface variations are distributed in both the normal and parallel fiber regions. On the other hand, the high temperature surface shows great variations in height between the normal and parallel fiber regions, with the normal fibers mostly at higher elevations from the nominal surface. Furthermore, deep groves appear at resin-rich locations, apparently

due to loss of the epoxy at the high temperature. A marked increase in the 10 point average height is also noted as the surface temperature is increased.

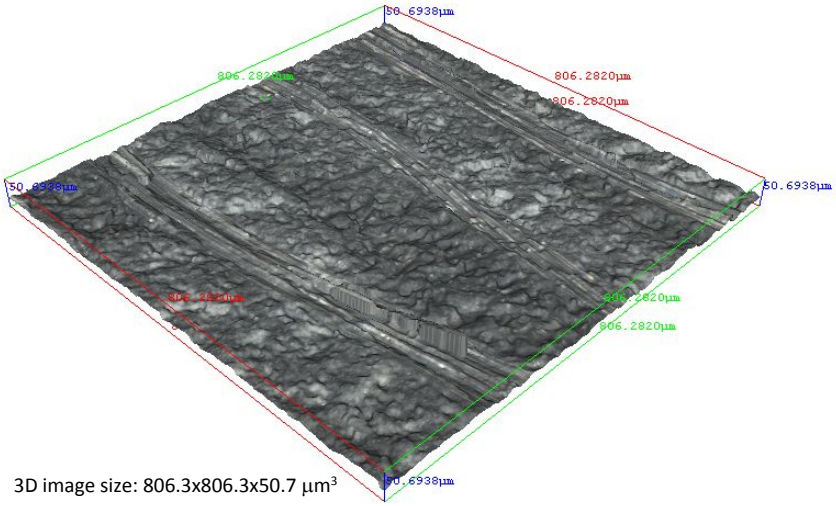

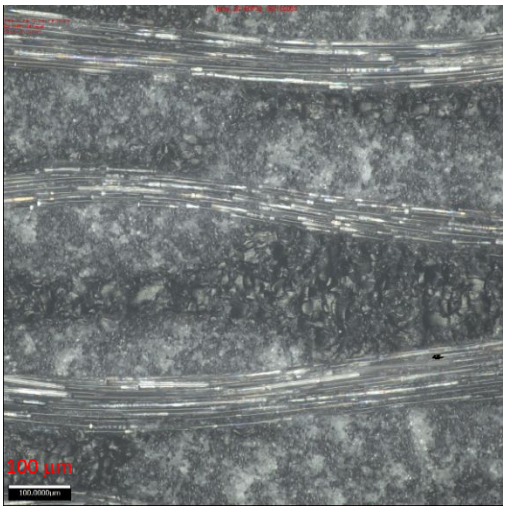

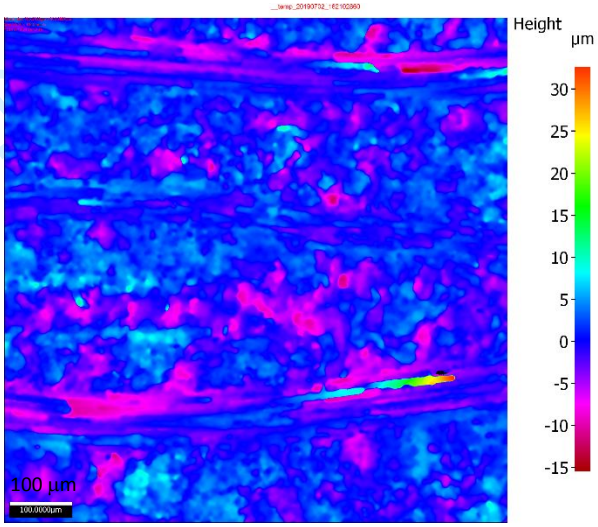

Figure 20. Surface texture of GFRP laminate after machining at 4000 rpm and 800 mm/min (T = 120 °C, S10z = 33.970±5.640 µm).

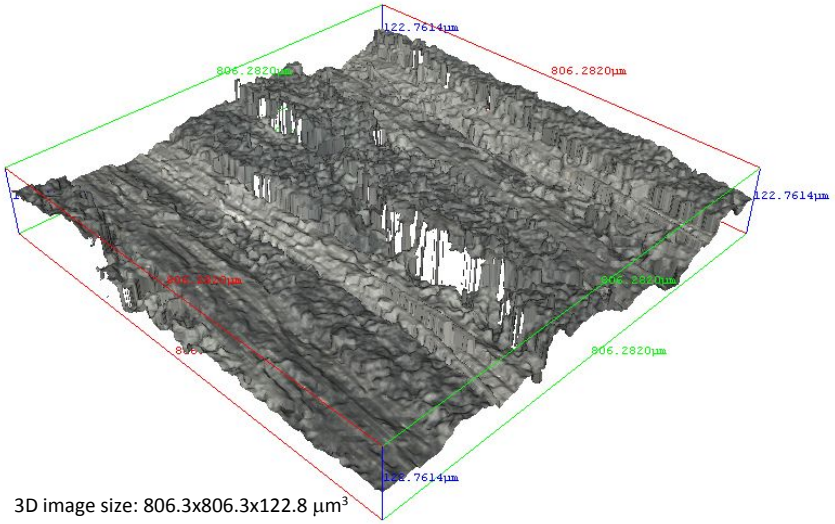

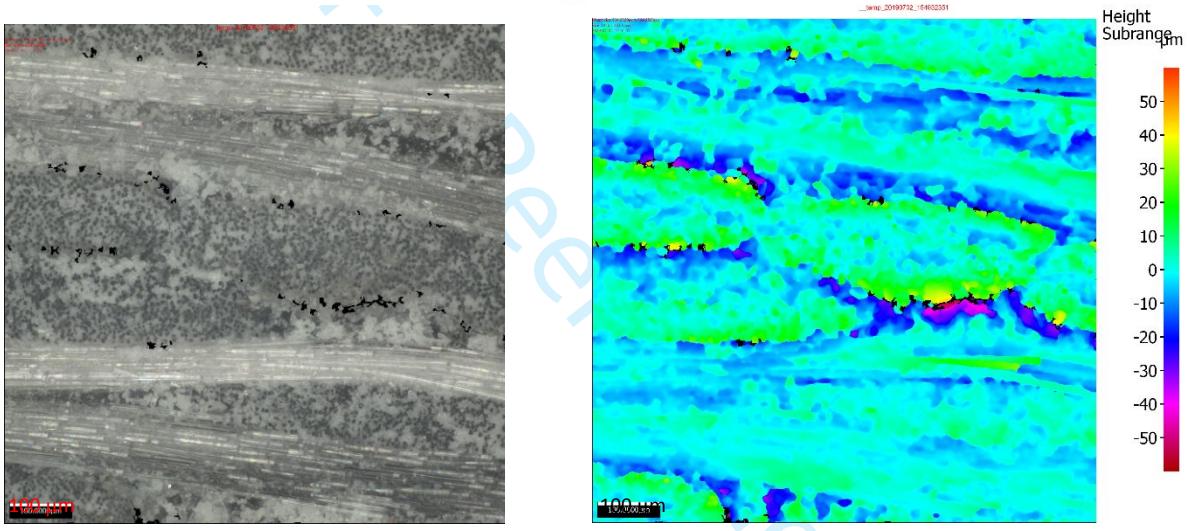

Figure 21. Surface texture of GFRP laminate after machining at 8000 rpm and 400 mm/min (T = 178 °C, S10z = 70.327±9.155 µm).

Conclusions

The heat partition problem in machining CFRP and GFRP with a two straight-flute PCD cutter was solved using the inverse heat conduction method. Three-dimensional numerical heat conduction models were used to represent the workpiece and cutting tool independently. The heat flux applied to each model was estimated by minimizing the difference between measured and calculated boundary temperatures. Conclusions drawn from this work are:

1. The heat partition problem in machining FRPs can be treated with reasonable accuracy using the inverse heat conduction method and by obtaining reliable boundary temperature measurements.
2. The bulk of the heat generated during machining (>86% for CFRP and >93% for GFRP) is conducted by the cutting tool and carried away by the chips. The portion of heat conducted to the laminate is very small (<14% for CFRP and <7% for GFRP).
3. The portion of heat conducted to the workpiece was more sensitive to changes in the feed speed than changes in the spindle speed. The largest heat partition to the workpiece occurs at the lowest feed speed and highest spindle speed (i.e. smallest feed per tooth).
4. The maximum temperature of the machined surface was estimated numerically and found to decrease with an increase in the feed per tooth for both laminate materials.
5. Surface texture of the machined edge did not vary considerably with machining conditions for the CFRP laminate. This is due to the fact that the maximum surface temperature was at or above the glass transition temperature (T_g = 180°C) for all cutting conditions.
6. Surface texture of the machined edge for the GFRP laminate varied greatly with feed per tooth. For the smallest feed per tooth where the machined surface temperature was the highest, the machined surface showed deep grooves in the resin-rich areas possibly due to the loss of matrix material.

References

[1] Shaw, M.C. Metal Cutting Principles, 2nd Ed. (2005) Oxford Universiy Press, Oxford, UK

[2] T. Inoue, M. Hagino. Cutting characteristics of CFRP materials with carbon fiber distribution. International Journal of Automation Technology (2013) 7(3):285-291

[3] Delahaigue, J., Chatelain, J.-F., Lebrun, G. (2017) Influence of Cutting Temperature on the Tensile Strength of a Carbon Fiber-Reinforced Polymer. Fibers, 5(4), 46. https://doi.org/10.3390/fib5040046

[4] Halim, N.F., Ascroft, H., Barnes, S. (2017) Analysis of Tool Wear, Cutting Force, Surface Roughness and Machining Temperature During Finishing Operation of Ultrasonic Assisted

Milling (UAM) of Carbon Fibre Reinforced Plastic (CFRP). Procedia Engineering 184: 185 – 191

[5] Sheikh-Ahmad, J.Y., Bailey, J.A. (1999) The wear characteristics of some cemented tungsten carbides in machining particleboard, Wear 225–229(1):256-266.

[6] Weinert, K. and Kempmann, C. (2004) Cutting Temperatures and Their Effects on the Machining Behaviour in Drilling Reinforced Plastic Composites. Advanced Engineering Materials 6(8):684-689.

[7] Khairusshima, M.K.N, Hassan, C.H., Jaharah, A.G., Amin, A.K.M., Idriss, A.N. (2013) Effect of chilled air on tool wear and workpiece quality during milling of carbon fibre-reinforced plastic. Wear 302:1113-1123.

[8] König, W. and Graß, P. Quality Definition and Assessment in Drilling of Fibre Reinforced Thermosets. Annals of the CIRP 38:1 (1989) 119-124.

[9] Liu, J., Chen, G., Ji, C., Qin, X., Li, H., & Ren, C. (2014). An investigation of workpiece temperature variation of helical milling for carbon fiber reinforced plastics (CFRP). International Journal of Machine Tools and Manufacture, 86, 89–103. https://doi.org/10.1016/j.ijmachtools.2014.06.008

[10] Hintze, W., Klingelhöller, C. Analysis and Modeling of Heat Flux into the Tool in Abrasive Circular Cutting of Unidirectional CFRP. Procedia CIRP 66 (2017) 210 – 214.

[11] Wang, F-J., Yin, J-W., Ma, J-W., Niu, B. Heat partition in dry orthogonal cutting of unidirectional CFRP composite laminates. Composite Structures 197 (2018) 28–38

[12] Sheikh-Ahmad, J. Y., Almaskari, F., Hafeez, F., Meng, F. Evaluation of heat partition in machining CFRP using inverse method. Machining Science and Technology, 23:4 (2019) 530-546. https://doi.org/10.1080/10910344.2019.1575401

[13] Kerrigan, K., O'Donnell, G. E. (2013). Temperature measurement in CFRP milling using a wireless tool-integrated process monitoring sensor. International Journal of Automation Technology, 7(6), 742–750.

[14] Ghafarizadeh, S., Lebrun, G. and Chatelain, J-F. "Experimental investigation of the cutting temperature and surface quality during milling of unidirectional carbon fiber reinforced plastic," J. Compos. Mater. 50:8 (2016) 1059-1071

[15] Yashiro, T., Ogawa, T., Sasahara, H. (2013). Temperature measurement of cutting tool and machined surface layer in milling of CFRP. International Journal of Machine Tools and Manufacture, 70, 63–69. https://doi.org/10.1016/j.ijmachtools.2013.03.009

[16] Wang, H., Sun, J., Zhang, D., Guo, K., & Li, J. (2016). The effect of cutting temperature in milling of carbon fiber reinforced polymer composites. Composites Part A: Applied Science and Manufacturing, 91, 380–387. https://doi.org/10.1016/j.compositesa.2016.10.025

[17] An, Q., Chen, J., Cai, X., Peng, T., Chen, M. (2018). Thermal characteristics of unidirectional carbon fiber reinforced polymer laminates during orthogonal cutting. Journal of Reinforced Plastics and Composites, 37(13), 905–916. https://doi.org/10.1177/0731684418768892

[18] Zhenyuan Jia, Rao Fu, Fuji Wang, Baowei Qian, Chunling He. Temperature Effects in End Milling Carbon Fiber Reinforced Polymer Composites. Polymer Composites 39:2 (2018) 437-447.

[19] J.L. Merino-Pérez, R. Royer, S. Ayvar-Soberanis, E. Merson, A. Hodzic. On the temperatures developed in CFRP drilling using uncoated WC-Co tools Part I: Workpiece constituents, cutting speed and heat dissipation. Composite Structures 123 (2015) 161–168.

[20] Khaled Giasin, Sabino Ayvar-Soberanis. Evaluation of Workpiece Temperature during Drilling of GLARE Fiber Metal Laminates Using Infrared Techniques: Effect of Cutting Parameters, Fiber Orientation and Spray Mist Application. Materials 2016, 9, 622; doi:10.3390/ma9080622

[21] Joven, R., Das, R., Ahmed, A., Roozbehjavan, P. and Minaie, B. “Thermal Properties of Carbon Fiber-Epoxy Composites With Different Fabric Weaves,” Sampe 2012 - Charleston, SC. October, 2012.

[22] Kalogiannakis, G., Van Hemelrijck, D., & Van Assche, G. (2004). Measurements of thermal properties of carbon/epoxy and glass/epoxy using modulated temperature differential scanning calorimetry. Journal of Composite Materials, 38(2), 163–175. https://doi.org/10.1177/0021998304038647

[23] Kerrigan, K., Thil, J., Hewison, R., O’Donnel, G.E. (2012) An Integral Telemetric Thermocouple Sensor for Process Monitoring of CFRP Milling Operations. Procedie CIRP 1:449-454.

[24] El-Hofy, H.H., Soo, S.L., Aspinwall, D.K., Sim, W.M., Pearson, D., M'Saoudi, R., Harden, P. (2017) Tool temperature in slotting of CFRP composites. Procedia Manufacturing 10:371-381.

[25] Sölter, J., & Gulpak, M. (2012). Heat partitioning in dry milling of steel. CIRP Annals - Manufacturing Technology, 61(1), 87–90. https://doi.org/10.1016/j.cirp.2012.03.046

[26] Luchesi, V. M., & Coelho, R. T. (2012). An inverse method to estimate the moving heat source in machining process. Applied Thermal Engineering, 45–46, 64–78. https://doi.org/10.1016/j.applthermaleng.2012.04.014